Progress In Electromagnetics Research Letters, Vol. 22, 29–38, 2011

SELF-FOCUSED PULSES IN TWO-DIMENSIONAL COMPOSITE RIGHT- AND LEFT-HANDED TRANSMISSION LINES WITH REGULARLY SPACED SCHOTTKY VARACTORS

J. Ogasawara and K. Narahara

Graduate School of Science and Engineering
Yamagata University
4-3-16 Jonan, Yonezawa, Yamagata 992-8510, Japan

Abstract—We experimentally characterize the pulse propagation in a two-dimensional composite right- and left-handed transmission line, whose shunt capacitors are replaced with the Schottky varactors. A properly designed line structure should produce that nonlinearity rendered by the varactors creating a self-focused pulse on the line and finally collapses, which allows it to be engineered for pulse processing systems. We built a test breadboard circuit and observed self-focused pulses.

1. INTRODUCTION

Composite right- and left-handed (CRLH) transmission lines have been intensively investigated to produce important breakthroughs in the management of electromagnetic continuous waves [1] in both one and two spatial dimensions. Several investigations have been done for managing dispersion [2–5] and for introducing nonlinearity to develop time-invariant envelope pulses [6, 7]. In particular, the 2D CRLH lines exhibit extraordinary refractive properties [8]. The highly dispersive nature of CRLH lines suits the development of electrical nonlinear Schrödinger (NS) solitons. In particular, the 2D NS equation has no stable spatially localized soliton solutions because its nonlinearity cannot be balanced with the dispersion under any conditions [9]. It is impossible to develop soliton-like pulses in any systems governed by 2D NS equation. Because diode currents screen

Received 19 January 2011, Accepted 21 March 2011, Scheduled 23 March 2011
Corresponding author: Koichi Narahara (narahara@yz.yamagata-u.ac.jp).

voltage waves in the forward-biased regions of shunt varactors, self-focusing due to the nonlinearity occurs only at reversely-biased voltage levels. This restricted nonlinearity might restore the balance between the nonlinearity and dispersion. A simplified line model validated this expectation through numerical evaluations. Management of the localized pulse can realize a variety of pulse control devices, including splitters, switches, variable delay rendering, and an i/o separator [10]. For these applications, it is important to observe the self-focused pulses in 2D Schottky CRLH lines.

First, we briefly review the fundamentals of 2D Schottky CRLH lines, including the configuration and the dispersion/nonlinearity coefficients of the 2D NS equation. Recently, we discussed line properties using the second-order accurate long-wavelength approximation [10]. However, the discrepancy between the approximated and exact dispersions is very large at short wavelengths for the formulation to describe the properties of short solitonic pulses. We improved the design criteria by applying the sixth-order long-wavelength approximation. Next, we discuss the results of several experiments, including those with self-focused pulse waveforms, and examine how much the focused pulse depends on the input amplitude and carrier frequency. To validate the circuit's operation principles, it is desirable that we can fix erroneous operations by reformation of the test circuit and detect easily voltages at any cells. We thus employ a standard breadboard. As a penalty of advantages, the experiments had to be carried out at MHz frequencies, being much smaller than microwave frequencies at which CRLH lines are vastly utilized.

2. FUNDAMENTAL PROPERTIES OF 2D SCHOTTKY CRLH LINES

Figure 1 shows the unit cell of the 2D Schottky CRLH line, where L_R, C_L, and L_L are the series inductance, series capacitance, and shunt inductance, respectively. The shunt capacitance C_R is given by Schottky varactors. Using C_L, we can set the required bias voltage for each cell (V_0 in Fig. 1). The dependence of the capacitance on the line voltage V is given by

$$C_R(V) = C_0 \left(1 - \frac{V}{V_J}\right)^{-m}, \tag{1}$$

where C_0, V_J, and m are the zero-bias junction capacitance, junction potential, and grading coefficient, respectively. The capacitance at $V = -V_0$, which we hereafter denote as $C_R^{(0)}$, determines the linear

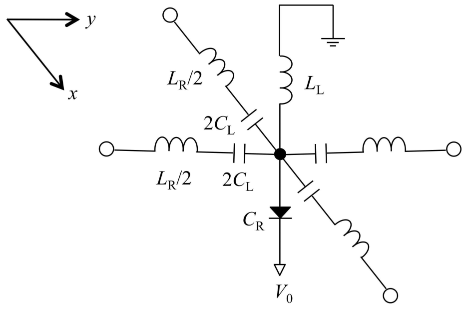

Figure 1. Unit cell of 2D Schottky CRLH line. The presence of C_L allows individual biasing of shunt varactors.

dispersion of the line, which is given by

$$\begin{aligned}\omega(k_x,k_y) = & \frac{1}{12\sqrt{5C_LC_R^{(0)}L_LL_R}}\Big[360(C_R^{(0)}L_L+C_LL_R)+C_LL_L \\ & \times\left(360k_x^2-30k_x^4+k_x^6+360k_y^2-30k_y^4+k_y^6\right) \\ & \mp\Big[-518400C_LC_R^{(0)}L_LL_R+360\left(C_R^{(0)}L_L+C_LL_R\right)+C_LL_L \\ & \times\left(360k_x^2-30k_x^4+k_x^6+360k_y^2-30k_y^4+k_y^6\right)^2\Big]^{1/2}\Big]^{1/2}, \quad (2)\end{aligned}$$

where $\omega(k_x,k_y)$ is the angular frequency of the wave specified by the wave vector $(k_x,\ k_y)$. In Eq. (2), the minus and plus at the head of the 3rd line correspond to the left- and right-handed branches, respectively. For convenience, *cells* are used as a spatial unit in this paper, because it allows the use of the per-unit-cell quantities such as C_L and L_R in the following expressions. Evaluating ω_{RH} and ω_{LH} at $k_x = k_y = 0$, the upper and lower transition frequencies of the CRLH line are given by $\omega_u = \max(1/\sqrt{C_LL_R}, 1/\sqrt{C_R^{(0)}L_L})$ and $\omega_l = \min(1/\sqrt{C_LL_R}, 1/\sqrt{C_R^{(0)}L_L})$, respectively. For the Schottky varactors, the capacitance decreases as V_0 increases. At sufficiently large V_0, the condition $C_R^{(0)}L_L < C_LL_R$ is satisfied. When V_0 decreases, ω_u decreases while ω_l is fixed until ω_u becomes equal to ω_l. As V_0 decreases more, ω_l starts to decrease while ω_u is fixed.

By introducing the spatial continuous variables x and y, and replacing the differences by differentials, the function $V = V(x,y,t)$ becomes the continuous counterpart of the voltage at the (i,j)th cell V_{ij}. For the reductive perturbation [11], we prepare spatial and temporal coordinates for the envelope and carrier waves. We use x, y, and t as the spatial and temporal coordinates, respectively, to describe the carrier wave. For the envelope wave, $\xi \equiv \epsilon(x - V_g t)$, $\eta \equiv \epsilon(y - U_g t)$, and $\tau \equiv \epsilon^2 t$ are used as the spatial and temporal coordinates, where V_g and U_g are given by $\partial_{k_x}\omega(k_x, k_y)$ and $\partial_{k_y}\omega(k_x, k_y)$, respectively, where $\omega = \omega(k_x, k_y)$ denotes the dispersion. We then expand the voltage variable as

$$V = \sum_{m=1}^{\infty} \epsilon^m \sum_{l=-\infty}^{\infty} u_l^{(m)}(\xi, \eta, \tau) e^{il(k_x x + k_y y - \omega t)}. \tag{3}$$

As a result, we obtain the following two-dimensional NS equation that describes $u_1^{(1)}$,

$$i\frac{\partial u_1^{(1)}}{\partial \tau} + p_1 \frac{\partial^2 u_1^{(1)}}{\partial \xi^2} + p_2 \frac{\partial^2 u_1^{(1)}}{\partial \xi \partial \eta} + p_3 \frac{\partial^2 u_1^{(1)}}{\partial \eta^2} + q \left| u_1^{(1)} \right|^2 u_1^{(1)} = 0, \tag{4}$$

where the dispersion coefficients p_1, p_2, and p_3 are given by $-\partial_{k_x}^2 \omega(k_x, k_y)/2$, $-\partial_{k_x}\partial_{k_y}\omega(k_x, k_y)$, and $-\partial_{k_y}^2 \omega(k_x, k_y)/2$, respectively, and the nonlinearity coefficient q is given by

$$q = \frac{90mC_R^{(0)} L_L \omega(-1 + C_L L_R \omega^2)}{(V_0 + V_J)^2} \frac{N(k_x, k_y)}{D(k_x, k_y)}, \tag{5}$$

where

$$\begin{aligned} N(k_x, k_y) &= -45(1+m) + 4\Big(45C_R^{(0)} L_L + C_L\big(4\big(45\left(k_x^2 + k_y^2\right) \\ &\quad -15\big(k_x^4 + k_y^4\big) + 2\big(k_x^6 + k_y^6\big)\big)L_L + 45L_R\big)(1+m)\Big)\omega^2 \\ &\quad -720 C_L C_R^{(0)} L_L L_R \omega^4, \end{aligned} \tag{6}$$

$$\begin{aligned} D(k_x, k_y) &= \Big(45 - 4\big(45C_R^{(0)} L_L + 4C_L\big(45\left(k_x^2 + k_y^2\right) - 15\left(k_x^4 + k_y^4\right) \\ &\quad +2\left(k_x^6 + k_y^6\right)\big)L_L + 45C_L L_R\big)\omega^2 + 720 C_L C_R^{(0)} L_L L_R \omega^4\Big) \\ &\quad \times\Big(-C_L\left(360\left(k_x^2 + k_y^2\right) - 30(k_x^4 + k_y^4) + k_x^6 + k_y^6\right)L_L \\ &\quad -360 C_L L_R + 360 C_R^{(0)} L_L\left(-1 + 2C_L L_R \omega^2\right)\Big), \end{aligned} \tag{7}$$

where $\omega = \omega(k_x, k_y)$ (See Ref. [7] for detailed derivation).

For the development of self-focused pulses traveling in the y orientation, q must have the same sign as p_1 and p_3. Fig. 2 shows the sample frequency dependence of the dispersive and nonlinearity coefficients. We set $C_0 = 64.77\,\mathrm{pF/cell}$, $V_J = 3.561\,\mathrm{V}$ and $M = 1.259$ to simulate a TOSHIBA 1SV101 varactor. The bias voltage V_0 was

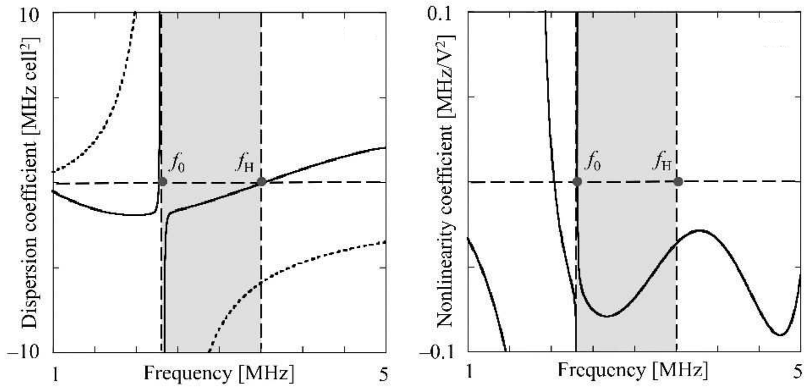

(a) (b)

Figure 2. Dispersion and nonlinearity coefficients of 2D Schottky CRLH lines. (a) The dispersion and (b) nonlinearity coefficients for $k_x = 0$. The dotted and solid curves in Fig. 2(a) show p_1 and p_3, respectively.

set to 1.0 V, C_L was set to 47 pF · cell, and L_R and L_L were set to 100 μH/cell and 100 μH · cell, respectively. For these parameters, the line becomes balanced, i.e., $\omega_u = \omega_l$ at $V_0 = 1.0$ V. The unique transition frequency is calculated to be 2.3 MHz. Fig. 2(a) shows the dispersion coefficients for $k_x = 0$. The dotted and solid curves represent p_1 and p_3, respectively. Note that p_2 is always zero for $k_x = 0$. Fig. 2(b) shows the nonlinearity coefficient. For frequencies from f_0 (2.3 MHz) to f_H (3.5 MHz), all three coefficients become negative; therefore, the pulse is expected to be self-focused at these frequencies.

3. EXPERIMENTAL OBSERVATIONS

We built a 45 × 35-cell 2D Schottky CRLH line on a standard breadboard. The Schottky varactors are TOSHIBA 1SV101 diodes. Shunt inductances and series capacitances were implemented using 100 μH inductors (TDK EL0405) and 47 pF capacitors (TDK FK24C0G1), respectively. The wavenumber is calculated to be 0.53 rad/cell for the 3.0-MHz wave propagating in the y orientation; therefore, the electrical lengths are 23.9 and 18.6 radians for the x and y orientations, respectively. As a result, the wave velocity is much smaller than the free-space light velocity. The middle 13 cells at the left boundary of the test line were fed by a pulse signal generated by an Agilent 81150A function generator, as shown in Fig. 3(a). An envelope pulse with a triangle waveform whose pulse width was set

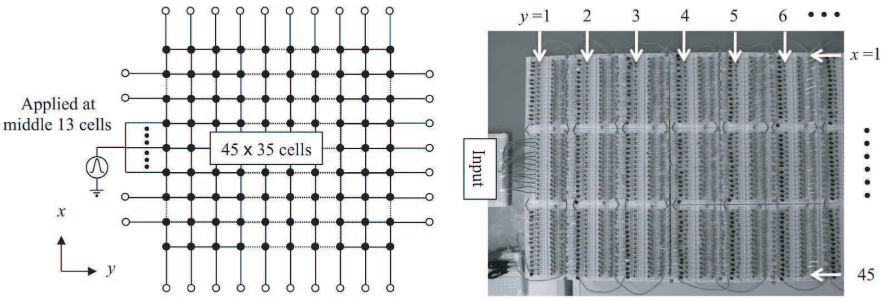

(a) (b)

Figure 3. Structure of the test 2D Schottky CRLH line. (a) The signal application and (b) the photo of the test circuit. The test line consists of 45 and 35 cells in the x and y orientations, respectively. An identical envelope pulse is applied to the middle 13 cells at the left edge.

to include 20 cycles of carrier sinusoidal wave was input. The signals along the test line were detected by Agilent 10073C passive probes and monitored in the time domain by using an Agilent DSO90254A oscilloscope. Fig. 3(b) shows the top-view photo of the test circuit. The circuit has 252 and 1925 millimeters long in the x and y orientations, respectively.

We examined the differences in the test line response to the input signal amplitude. As shown in Fig. 2, we set the carrier frequency to 3.0 MHz, where we expect the self-focusing to occur. First, we measured the response to small signal inputs. The amplitude of the input pulse was set to 0.5 V. Fig. 4(a) shows the spatial pulse profile recorded when the input pulse becomes maximal at the left edge. Figs. 4(b), (c), and (d) show the profiles recorded at succeeding points in increments of 0.05 μs. As expected, the peak travels in the $+y$ direction and its spread is almost unaltered. Moreover, the peak amplitude decreases due to attenuation and diffusion.

On the other hand, Figs. 4(e), (f), (g), and (h) show the profiles for the large amplitude input signals recorded at the same timing as Figs. 4(a), (b), (c), and (d), respectively. To obtain these profiles, we set the amplitude of input pulse to 3.0 V. In contrast to the linear case, the peak amplitude increases with a reduced spread.

In order to see this more clearly, Fig. 5(a) shows the profiles in the x orientation for y in $[1, 6]$, where we recorded the maximum voltage observed in the measured temporal span of each cell for a large amplitude input. The voltage spread clearly converges to the

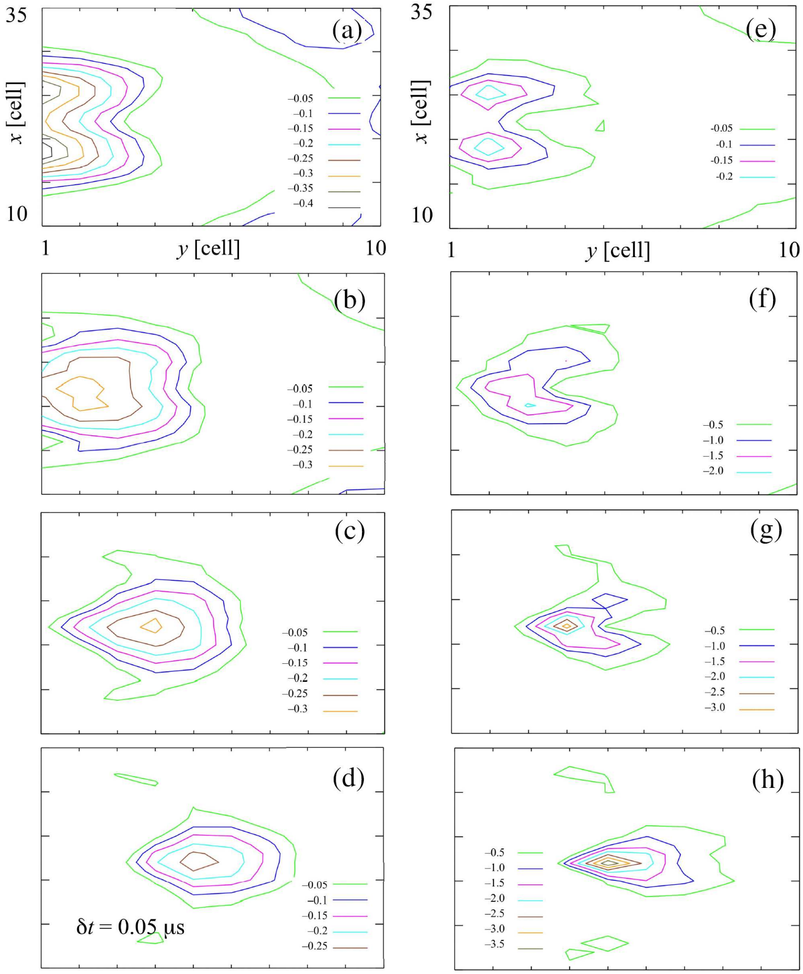

Figure 4. Pulses in the 2D Schottky CRLH line. Spatial pulse profiles are shown in $[10, 35] \times [1, 10]$. Some profile divisions are omitted for clarity, but they are identical with those in Figs. 4(a) and (e). Figs. 4(a), (b), (c), and (d) present spatial profiles for small amplitude inputs and Figs. 4(e), (f), (g), and (h) present profiles for large amplitude inputs.

central cell. Fig. 5(b) shows the profile at $x = 23$ in the y orientation. The figure shows the maximum voltage of each cell, normalized by that of the input cell, which is considered as a good indicator of self-focusing. The solid and dotted curves correspond to the profiles for large and small amplitude inputs, respectively. The solid curve exhibits

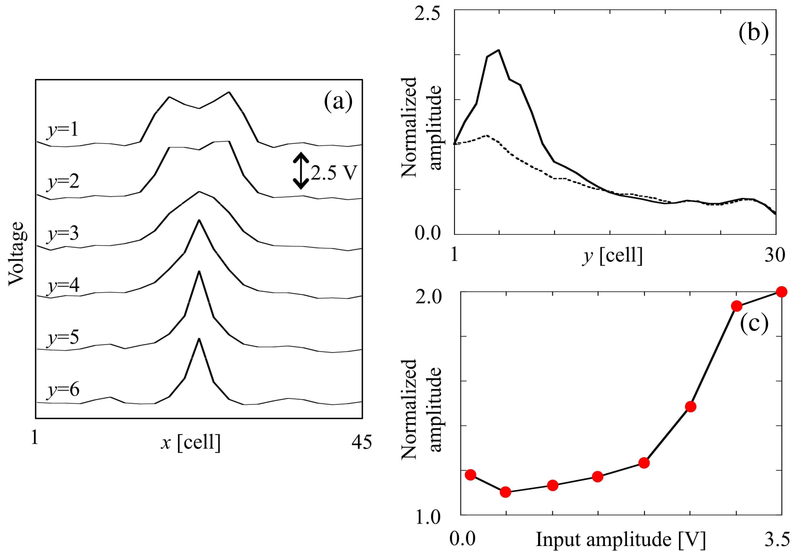

Figure 5. Self-focusing observed in the test 2D Schottky CRLH line. (a) The voltage profile in the x orientation, (b) the normalized amplitude profile in the y orientation and (c) the dependence of the normalized amplitude on the input amplitude. The normalized amplitude is the peak amplitude divided by that of the input.

a remarkable increase up to $y = 5$. Note that the normalized amplitude becomes twice as large as the input at $y = 5$. At $5 < y < 15$, the amplitude decays relatively steeper than the small amplitude profile, and becomes so small that nonlinearity is weakened, resulting into the two profiles becoming almost identical at $y \geq 15$. The dependence of the maximum normalized amplitude on the input pulse amplitude is shown in Fig. 5(c). For small inputs having 1.0 V at most, the maximum normalized amplitude is almost unity. It drastically increases at larger inputs.

Finally, we examine the carrier frequencies where the self-focused pulse can develop for varactors biased at several different voltages. The lower and upper limits for self-focusing are represented by the circles and the squares, respectively, in Fig. 6. Analytically, self-focused pulses can develop only for carrier frequencies $\in (f_0,\ f_H)$. The solid and dashed curves in Fig. 6 show the locations of f_0 and f_H, respectively, and the measured self-focused pulses satisfy the analytical requirement. Moreover, the measured lower limit frequencies are well explained by f_0.

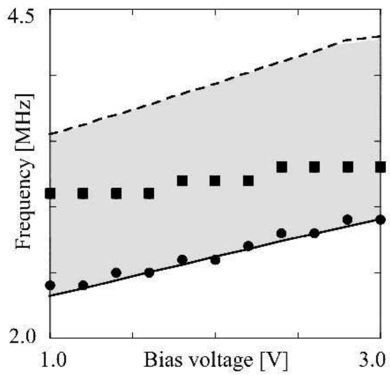

Figure 6. Carrier frequencies for developing self-focused pulses. The solid and dashed curves show the locations of f_0 and f_H, respectively, and the shaded region corresponds to carrier frequencies where p_1, p_3 and q have a common sign. Self-focused pulses were observed at the frequencies between the circles and squares.

4. CONCLUSION

We measured a test 2D Schottky CRLH line to investigate the development of self-focused pulses and clarify how the pulse properties depend on the carrier frequency, bias voltage, and the input amplitude. Moreover, the dispersion and nonlinearity coefficients of the nonlinear Schrödinger equation derived by the reductive perturbation accurately give the conditions for the development of self-focused pulses. Although we cannot observe a stable propagation of localized pulses due to large parasitic resistance of the inductors, it should be possible when employing low-loss platforms, such as printed circuit boards and integrated circuits.

REFERENCES

1. Caloz, C. and T. Itoh, *Electromagnetic Metamaterials: Transmission Line Theory and Microwave Applications*, Wiley, 2006.
2. Monti, G. and L. Tarricone, "Gaussian pulse expansion of modulated signals in a double-negative slab," *IEEE Trans. Microwave Theory and Techniques*, Vol. 54, 2006.
3. Monti, G. and L. Tarricone, "Signal reshaping in a transmission line with negative group velocity behaviour," *Microwave Optical Technol. Lett.*, Vol. 51, 2627–2633, 2009.
4. Chi, P. and T. Itoh, "Dispersion engineering with CRLH

metamaterials," *Proc. IEEE International Symposium on Radio-frequency Integration Technology*, 128–131, 2009.

5. Gómez-Diaz, J. S., S. Gupta, A. Álvarez-Melcón, and C. Caloz, "Investigation on the phenomenology of impulse-regime metamaterial transmission lines," *IEEE Trans. Antennas and Propagat.*, Vol. 57, 4010–4014, 2009.
6. Gharakhili, F. G., M. Shahabadi, and M. Hakkak, "Bright and dark soliton generation in a left-handed nonlinear transmission line with series nonlinear capacitors," *Progress In Electromagnetics Research*, Vol. 96, 237–249, 2009.
7. Ogasawara, J. and K. Narahara, "Short envelope pulse propagation in composite right- and left-handed transmission lines with regularly spaced Schottky varactors," *IEICE Electron. Express*, Vol. 6, 1576–1581, 2009.
8. Iyer, K. and G. Eleftheriades, "Free-space imaging beyond the diffraction limit using a Veselago-Pendry transmission-line metamaterial superlens," *IEEE Trans. Antennas and Propagat.*, Vol. 57, 1720–1727, 2009.
9. Gaponov-Grekhov, A. V. and M. I. Rabinovich, "L. I. Mandel'shtam and the modern theory of nonlinear oscillations and waves," *Sov. Phys. Usp.*, Vol. 22, 590–614, 1979.
10. Nakamichi, T., S. Nakagawa, and K. Narahara, "Management of spatially-localized pulses in two-dimensional composite right- and left-handed transmission lines periodically loaded with Schottky varactors," *Jpn. J. Appl. Phys.*, Vol. 47, 6583–6587, 2008.
11. Taniuti, T., "Reductive perturbation method and far fields of wave equations," *Prog. Theor. Phys. Suppl.*, Vol. 55, 1–55, 1974.